Electronic Supplementary Material (ESI) for Journal of Materials Chemistry A.

Supplementary Materials for

Bioinspired gradient-structured wood interfaces achieving efficient ion diffusion to generate electricity from natural evaporation

Chuanlong Han, ‡[ab] Ziqi Bai, ‡[ab] Huihong Sun,[ab] Lintao Mi, [ab] Zhuangzhi Sun[ab]*

[a] *Province Key Laboratory of Forestry Intelligent Equipment Engineering, College of Mechanical and Electrical Engineering, Northeast Forestry University, Harbin 150000, People's Republic of China.*

[b] *Key Laboratory of Biobased Material Science & Technology, Ministry of Education, Northeast Forestry University, Harbin 150000, People's Republic of China.*

‡ *These authors contributed equally to this work.*

* *Corresponding authors. Email: sunzhuangzhi@nefu.edu.cn*

Brief description of what this file includes:

Supplementary Fig. 1 Microstructure of wood before and after chemical treatment.

Supplementary Fig. 2 Evaporation rates in cellulosic wood, GO/CNT NFM, and tap water.

Supplementary Fig. 3 The electrochemical impedance along the OCG gradient.

Supplementary Fig. 4 Continuous short-circuit and power densities of W-IENG with the OCG gradient.

Supplementary Fig. 5 Characterizations and schematic diagram of the interfacial interaction of the Ml-GO/CNT interface.

Supplementary Fig. 6 Schematic diagram of the successive spinning method for different regions.

Supplementary Fig. 7 Corresponding analysis of the Ml-GO/CNT interface from EDS mapping results.

Supplementary Fig. 8 XPS spectrum of 1-side and 4-side at the Ml-GO/CNT interface.

Supplementary Fig. 9 Electrochemical analysis at different interfacial ratios of the OCG gradient.

Supplementary Fig. 10 Effect of water transport and evaporation capacity of multilayer structure on power output.

Supplementary Fig. 11 Mass change of evaporation of W-IENG with 4-OCG gradient at different migration distances.

Supplementary Fig. 12 SEM images and voltage outputs of the Ml-GO/CNT interface with different fiber diameters.

Supplementary Fig. 13 Loaded power generation performance of the W-IENG.

Supplementary Fig. 14 Evaporation and power generation performance of W-IENG in seawater over the long term.

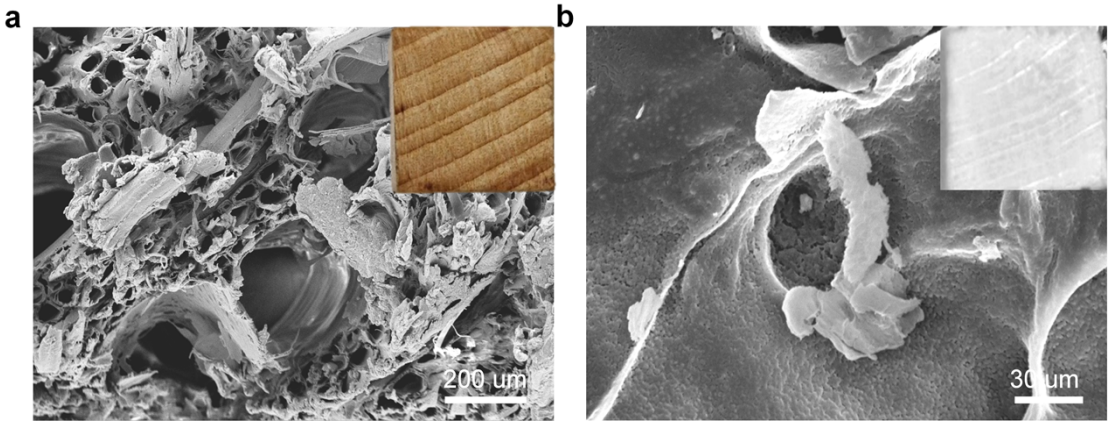

Fig. S1 Microstructure of wood before and after chemical treatment. (a) SEM images of the cross-section of native wood. Inset is a photograph of the native wood. (b) SEM images of the cross-section of a cellulosic wood. Inset is a photograph of the cellulosic wood.

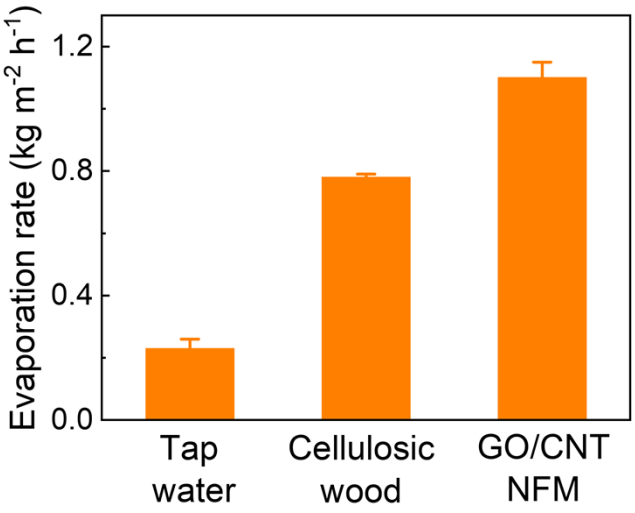

Fig. S2 Evaporation rates in cellulosic wood, GO/CNT NFMs, and tap water.

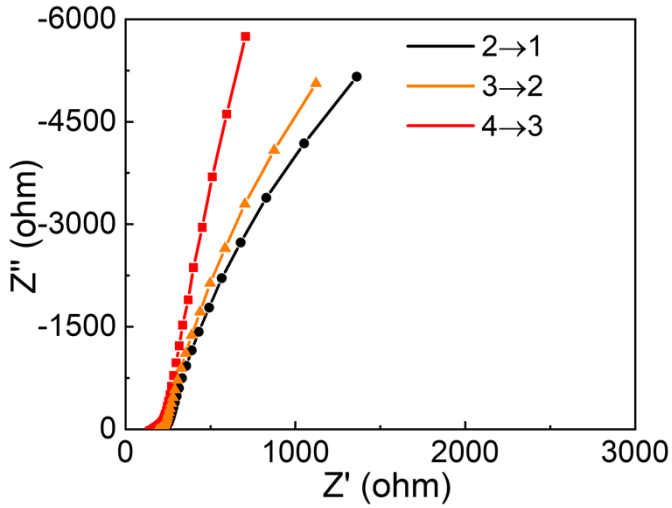

Fig. S3 The electrochemical impedance along the OCG gradient.

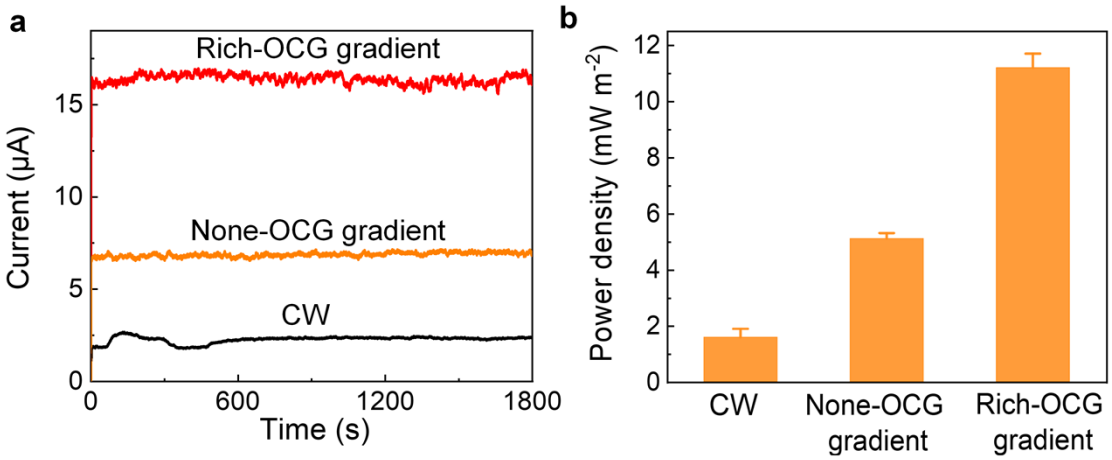

Fig. S4 Continuous short-circuit and power densities of W-IENG with the OCG gradient in seawater at one sun. (a) Continuous short-circuit. (b) Loaded power densities.

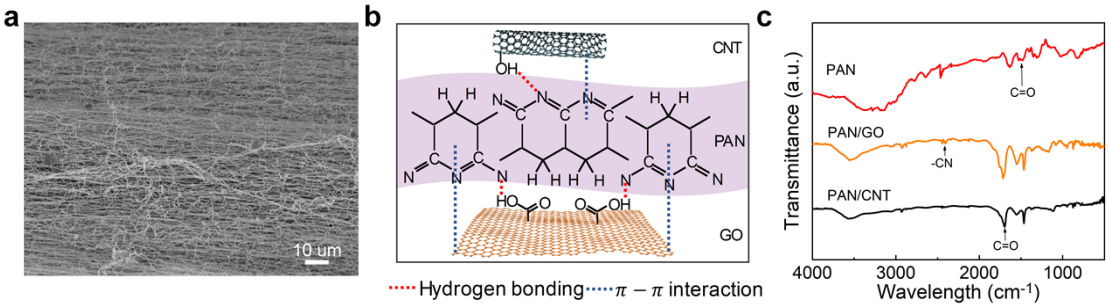

Fig. S5 Characterizations and schematic diagram of the interfacial interaction of the Ml-GO/CNT interface. (a) The multilayer structure cross-sectional SEM image of the Ml-GO/CNT interface. (b) Schematic diagram of the interfacial interaction between PAN and GO, CNT. (c) FT-IR spectra of PAN/GO, PAN/CNT, and PAN.

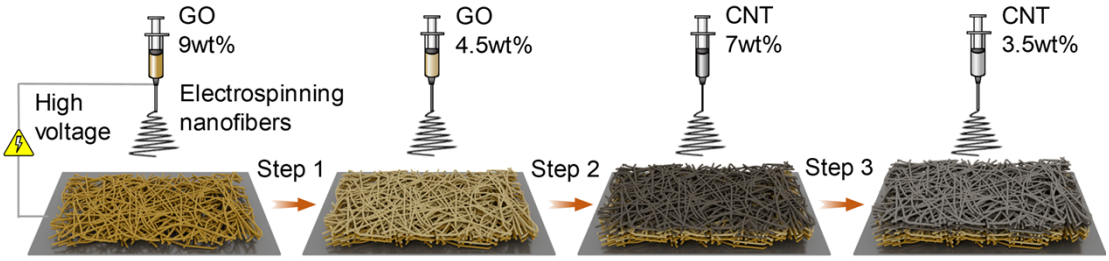

Fig. S6 Schematic diagram of the successive spinning method for different regions.

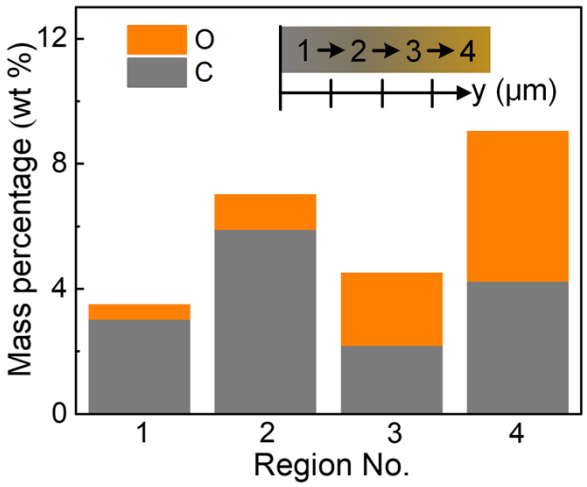

Fig. S7 Corresponding analysis of the Ml-GO/CNT interface from EDS mapping results.

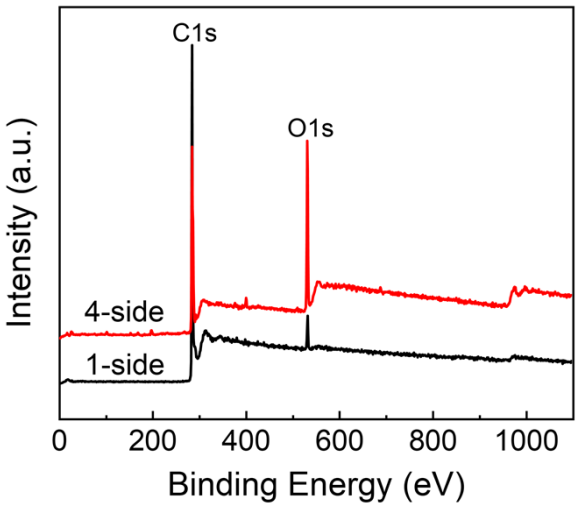

Fig. S8 XPS spectrum of 1-side and 4-side at the Ml-GO/CNT interface.

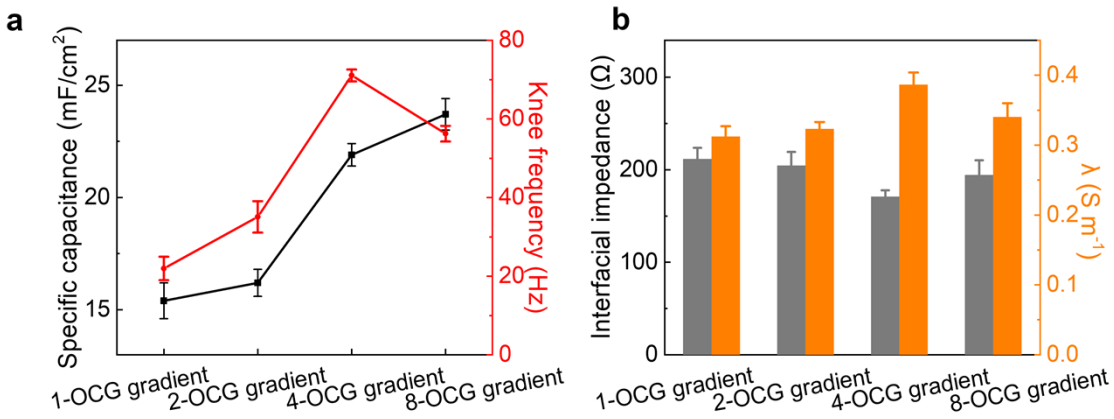

Fig. S9 Electrochemical analysis at different interfacial ratios of the OCG gradient. (a) Specific capacitance and knee frequency of OCG gradient with different interfacial ratios. (b) Interfacial impedance and conductivity of the OCG gradient with different interfacial ratios.

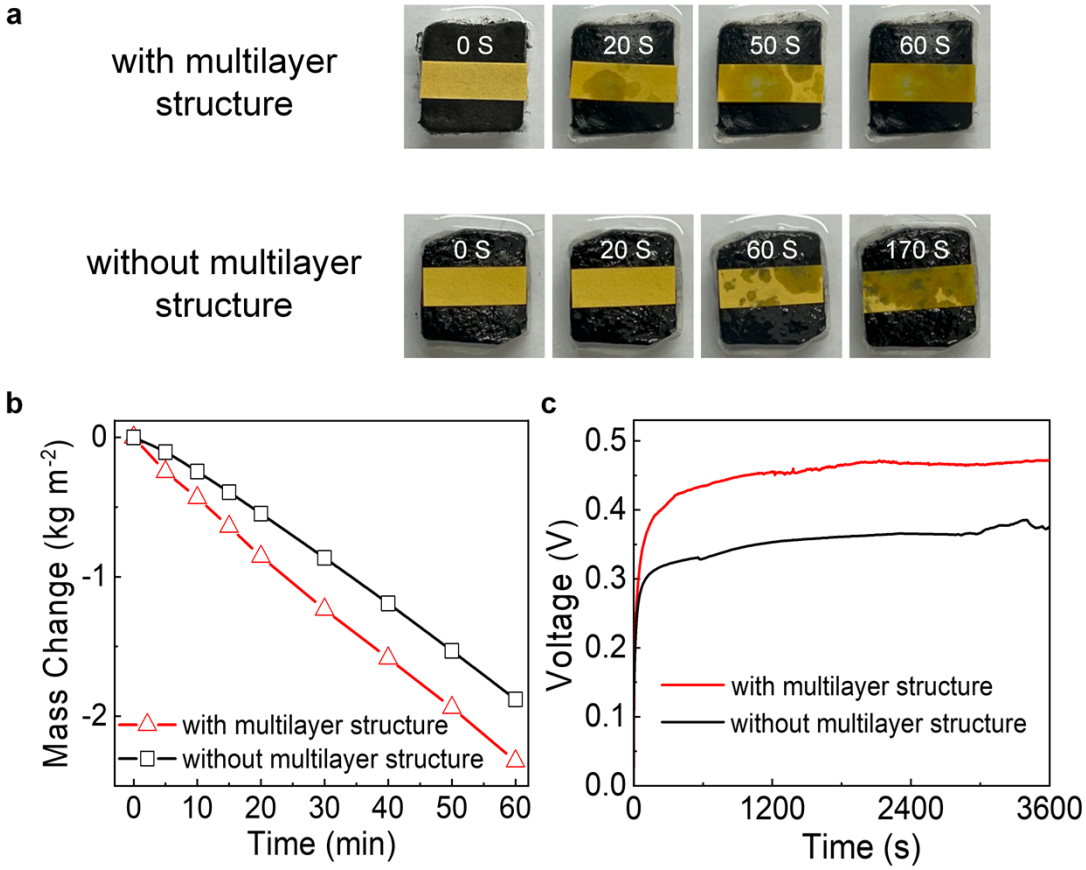

Fig. S10 Effect of water transport and evaporation capacity of multilayer structure on power output. (a) Upward water transport capacity, (b) Mass change of evaporation, c) Open-circuit voltage.

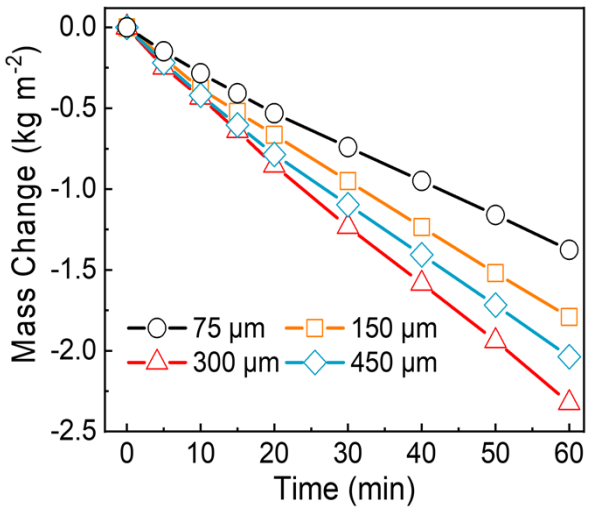

Fig. S11 Mass change of evaporation of W-IENG with 4-OCG gradient at different migration distances.

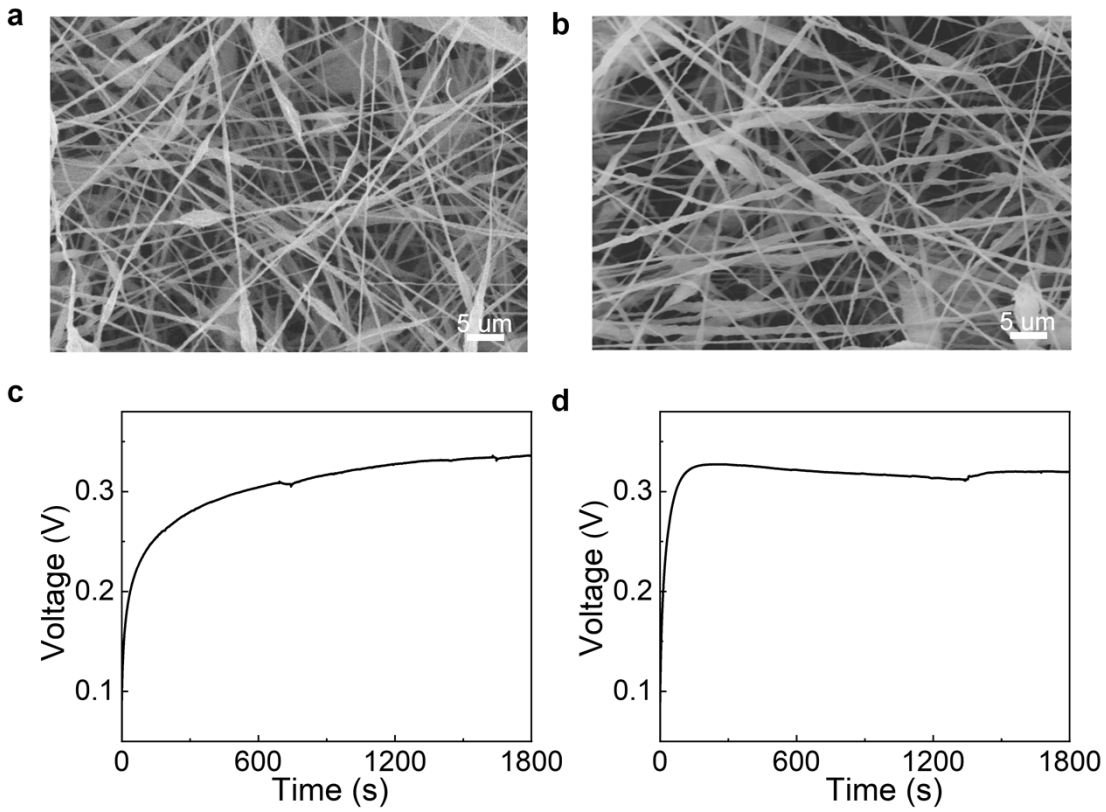

Fig. S12 SEM images and voltage outputs of the Ml-GO/CNT interface with different fiber diameters. **(**a, c) Average diameter around 350 nm. (b, d) Average diameter around 470 nm. The diameter of the fibers was adjusted by changing the voltage applied in the electrospinning process, and the applied voltages were 15 kV and 20 kV, respectively.

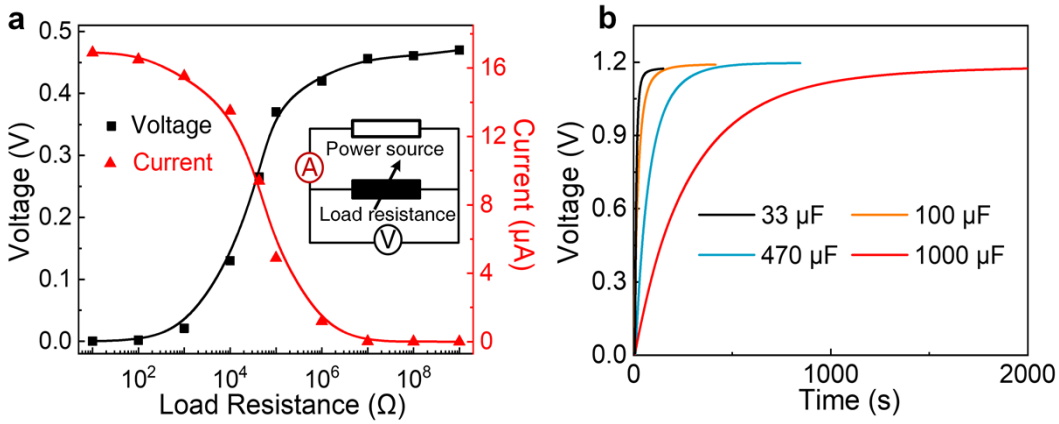

Fig. S13 Loaded power generation performance of the W-IENG. **(**a) Current and voltage generated by the W-IENG connected to a variable external load. (b) Voltage-time curves of commercial capacitors when charged by the integrated W-IENGs system.

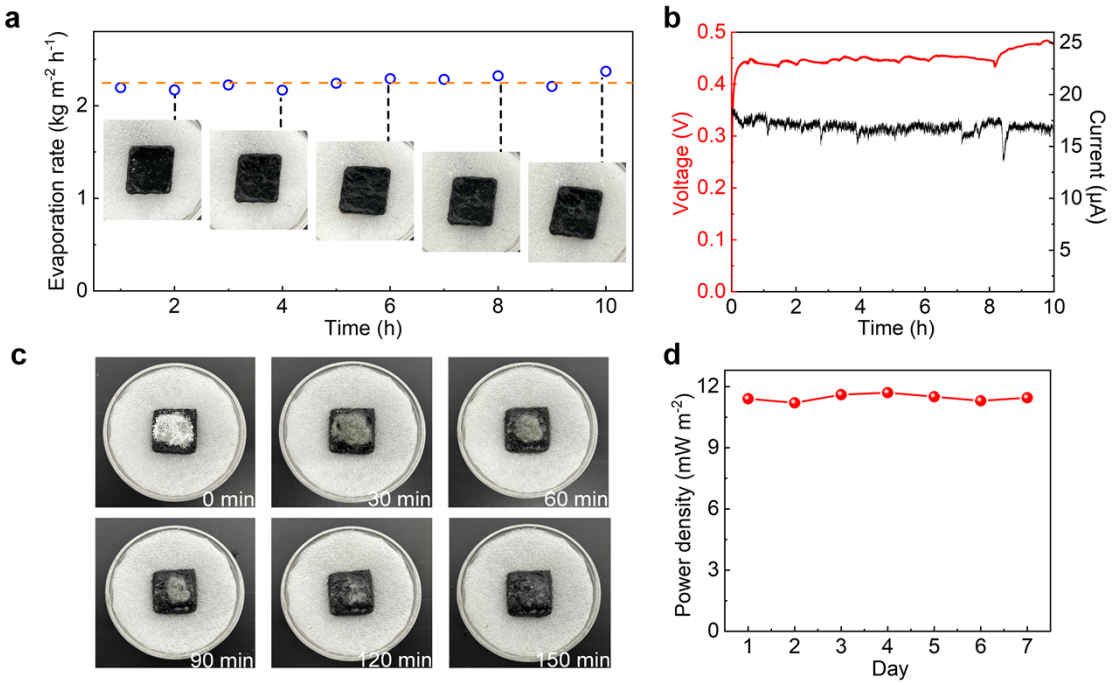

Fig. S14 Evaporation and power generation performance of W-IENG in seawater over the long term. (a) The variation of water evaporation rate with time under one sun in seawater. (b) Continuous voltage output and circuit current of W-IENG in seawater at one sun for about 10 h. (c) Self-cleaning process of W-IENG at night. (d) Output power of W-IENG immersed in seawater for 7 days.